Journal of Thermal Science Vol.31, No.1 (2022) 151−162

https://doi.org/10.1007/s11630-022-1564-2 **Article ID: 1003-2169(2022)01-0151-12**

Aerodynamic Performance Improvement of a Highly Loaded Compressor Airfoil with Coanda Jet Flap

ZHANG Jian[1], DU Juan[2,3,4,5*], ZHANG Min[2,3,4,5*], CHEN Ze[6], ZHANG Hongwu[2,3,4,5], NIE Chaoqun[2,3,4,5]

1. North China Electric Power University, Beijing 100096, China
2. Advanced Gas Turbine Laboratory, Institute of Engineering Thermophysics, Chinese Academy of Sciences, Beijing 100190, China
3. Key Laboratory of Advanced Energy and Power, Chinese Academy of Sciences, Beijing 100190, China
4. Innovation Academy for Light-Duty Gas Turbine, Chinese Academy of Sciences, Beijing 100190, China
5. School of Engineering Science, University of Chinese Academy of Sciences, Beijing 100190, China
6. Changsha University of Science & Technology, Changsha 410114, China

Abstract: Coanda jet flap is an effective flow control technique, which offers pressurized high streamwise velocity to eliminate the boundary layer flow separation and increase the aerodynamic loading of compressor blades. Traditionally, there is only single-jet flap on the blade suction side. A novel Coanda double-jet flap configuration combining the front-jet slot near the blade leading edge and the rear-jet slot near the blade trailing edge is proposed and investigated in this paper. The reference highly loaded compressor profile is the Zierke & Deutsch double-circular-arc airfoil with the diffusion factor of 0.66. Firstly, three types of Coanda jet flap configurations including front-jet, rear-jet and the novel double-jet flaps are designed based on the 2D flow fields in the highly loaded compressor blade passage. The Back Propagation Neural Network (BPNN) combined with the genetic algorithm (GA) is adopted to obtain the optimal geometry for each type of Coanda jet flap configuration. Numerical simulations are then performed to understand the effects of the three optimal Coanda jet flaps on the compressor airfoil performance. Results indicate all the three types of Coanda jet flaps effectively improve the aerodynamic performance of the highly loaded airfoil, and the Coanda double-jet flap behaves best in controlling the boundary layer flow separation. At the inlet flow condition with incidence angle of 5°, the total pressure loss coefficient is reduced by 52.5% and the static pressure rise coefficient is increased by 25.7% with Coanda double-jet flap when the normalized jet mass flow ratio of the front jet and the rear jet is equal to 1.5% and 0.5%, respectively. The impacts of geometric parameters and jet mass flow ratios on the airfoil aerodynamic performance are further analyzed. It is observed that the geometric design parameters of Coanda double-jet flap determine airfoil thickness and jet slot position, which plays the key role in supressing flow separation on the airfoil suction side. Furthermore, there exists an optimal combination of front-jet and rear-jet mass flow ratios to

Article type: Contributed by Asian Congress on Gas Turbines 2020 (August 18–19, 2021, China).
Received: Oct 15, 2021
Corresponding author: DU Juan; E-mail: dujuan@iet.cn
ZHANG Min zhangmin@iet.cn

achieve the minimum flow loss at each incidence angle of incoming flow. These results indicate that Coanda double-jet flap combining the adjust of jet mass flow rate varying with the incidence angle of incoming flow would be a promising adaptive flow control technique.

Keywords: Coanda jet flap, high loaded compressor, active flow control, aerodynamic performance

Nomenclature

ANN	Artificial Neural Network	R	Coanda surface radius
BPNN	Back Propagation Neural Network	R_1	Coanda surface radius near the trailing edge
CFD	Computational Fluid Dynamics	R_2	Coanda surface radius near the leading edge
C_{ax}	axial chord	SST	Shear Stress Transport
C_v	specific heat at constant volume	T	static temperature
C_p	static pressure coefficient	TE	trailing edge
$d\omega$	change in total pressure loss coefficient	t	time variable
$d(\Delta P_s)$	change in non-dimensional static pressure rise coefficient without Coanda jet	U	velocity
e	internal energy	y^+	non-dimensional wall distance
GA	Genetic Algorithm	α	angle of the point between Coanda curve and modified suction surface
h	jet sloth width	α_1	angle of the point between Coanda curve and modified suction surface
LE	Leading Edge	α_2	angle of the point between Coanda curve and modified suction surface
m_1	non-dimensional inlet mass flow rate	γ_i	ratio of specific heats
m_j	non-dimensional Coanda jet mass flow rate	θ	angle of the point between Coanda curve and suction surface
ΔP_s	non-dimensional static pressure rise coefficient without Coanda jet	θ_1	angle of the point between Coanda curve and trailing edge
ΔP_{sj}	non-dimensional static pressure rise coefficient with Coanda jet	θ_1	angle of the point between Coanda curve and leading edge
p	static pressure	κ	thermal conductivity
p_1	inlet static pressure	μ	dynamic viscosity of the air
p_2	outlet static pressure	ρ	air ideal density
p_i	blade surface static pressure	σ_{visc}	stress tensor
p_{t1}	inlet total pressure without Coanda jet	ω	total pressure loss coefficient
p_{t2}	outlet total pressure	ω_j	total pressure loss coefficient with Coanda jet
p_{tj}	total pressure of Coanda jet	2D	2-dimensional
p_{t1j}	inlet total pressure with Coanda jet	3D	3-dimensional
RANS	Renolds-Average Navier-Stokes		

1. Introduction

A pivotal aim of modern high-performance aeroengines is to improve the engine thrust-weight ratio. To realize this purpose, an applicable way is to increase the load of compressor rotor and stator blades. However, this will increase the flow turning angle, which could deteriorate the flow field in the compressor and hence lead to higher total pressure loss. Meanwhile, some design experience indicates that the diffusion factor of a compressor should not exceed 0.6 [1] to avoid severe flow separations. Therefore, various flow control techniques, such as air blowing [2], boundary layer suctions [3], casing treatments [4], and plasma actuations [5], have been investigated to improve the blade load and ensure a wide operation range for compressors.

Jet flap is also an effective flow control technique. It offers pressurized high-velocity air blowing to eliminate the boundary layer flow separation and increase the aerodynamic loading level. This flow control technique is originally proposed in external flow field to improve the lift coefficient for aircraft wings. As denoted by Day [6], the lift of an aircraft wing can be increased by 2 to 3 when using the jet flap. Due to this successful application, researchers are inspired to adopt the jet flap to improve the flow stability of compressors. Consequently, series of experimental and numerical investigations have been conducted to validate the control effectiveness of the jet flap.

The most pioneering work, where the jet flap was introduced into an axial compressor for the first time, was carried out by Edward [7]. Their experimental measurements demonstrated that the jet flap could increase the blade lift coefficient and enlarge the stall angle. Later, Landsberg et al. [8] analyzed the influences of normal blowing and tangential blowing for the jet flap that was constructed near the trailing edge of a compressor blade. They pointed out that the tangential blowing achieved higher efficiency than the normal case. Despite this, installing the jet flap along the tangential direction may destroy the continuity of the blade profile. This could lead to negative effects on the compressor performance and hence weakens the positive impacts of the jet flap.

In order to conquer the above issues, the Coanda effect [9] is combined with the jet flap to generate "Coanda jet", its essence lies in a fact that the Coanda jet flow is easy to attach a curved wall when it is introduced along the tangential direction of the surface. This is ascribed to a decrease in static pressure near the wall. Therefore, the Coanda jet can aid to realize a significant change in the flow direction within a short distance.

Hill [10] performed a two-dimensional (2D) numerical simulation for a circulation control IGV that took advantage of the Coanda jet for flow vectoring. Fischer [11] adopted the Coanda jet to the first-stage stator of a four-stage high-speed axial compressor and successfully reduced the stator solidity. Vorreiter [12] further denoted that effect of the extra energy from the injected flow should be considered and they suggested that the blowing mass ratio should be less than 1.5%. In addition, the impacts of the Coanda jet on the three-dimensional (3D) flow field of a compressor were studied by Fischer [13], and results implied that the blade number could be reduced by 20% without performance deficits when the diffusion factor was increased from 0.52 to 0.56. Also, for the high-speed compressor investigated by Guendogdu [14], employing the Coanda jet with a blowing ratio of 0.5% could reduce the stator solidity by 25%. Moreover, Schwerdt [15] confirmed via experiments that the stator Coanda jet inhibited flow separations in a four-stage axial compressor, where hub aspirations were simultaneously applied.

All of the above woks certified that the Coanda jet is beneficial to improve compressor performance. However, most of them focus on compressors with low turning angle blades. Rare studies in the open literature evaluate the effectiveness of the Coanda jet for highly loaded compressors. Therefore, the effects of the Coanda jet flap on the performance of those types of compressors are still obscure, and relevant design criteria need to be established to proceed the application of the Coanda jet flap in modern aeroengines.

Considering the above situations, the Coanda jet effects on the performance of highly loaded compressors are systematically investigated in the present study. This paper is organized as follow. The key geometric parameters of the reference airfoil and three initial Coanda jet flap designs are firstly introduced in Section 1. Then, the genetic algorithm [16] in conjunction with an artificial neural network is adopted to design the optimal aerodynamic shape of two types of jet slots in Section 2. The flow fields in a highly loaded compressor airfoil under various incoming Mach number conditions are firstly investigated in Section 3. In Section 4, the mechanism of those Coanda jet slots and the blowing ratios to control the boundary layer separation is clarified. The primary purpose is to establish a stable and efficient design optimization platform of the Coanda jet flap for highly loaded compressors. Also, those works provide a quantitative evaluation of the Conanda jet flap under various Mach number conditions, and this aids to offer a guideline for adaptive flow control techniques.

2. Reference Compressor Cascade and Coanda Jet Flap Geometry

The Zierke & Deutsch airfoil [16] with a double-circular-arc profile is selected here as the reference compressor cascade and its key geometric parameters are listed in Table 1. This cascade is highly

Table 1 Zierke & Deutsch profile key parameters

Parameter	Value
Chord length	228.6 mm
Pitch Width	106.8 mm
Solidity	2.14
Stagger angle	20.5°
Camber angle	65.0°
Aspect ratio	1.61
Inlet metal angle	53°
Outlet metal angle	12°

loaded with a diffusion factor of 0.66 at the design point. In this paper, the Zierke & Deutsch airfoil is scaled down by a ratio of 1:2.83 as conducted in the convenience of the subsequent test verification study.

Three types of Coanda jet flap are designed here. They include two single Coanda jet slot close to the trailing edge and the leading edge respectively, and a combined Coanda jet slots close to both the trailing and leading edges. Schematic diagram of the Zierke & Deutsch airfoil and three Coanda jet configurations are shown in Fig. 1. All jet slots are constituted on the blade suction surface to realize tangential blowing, while profile of the blade pressure surface, radius of both leading edge and trailing edge are not changed.

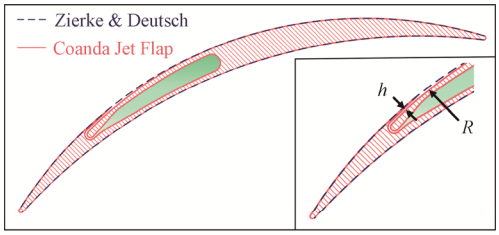

(a) Front-jet

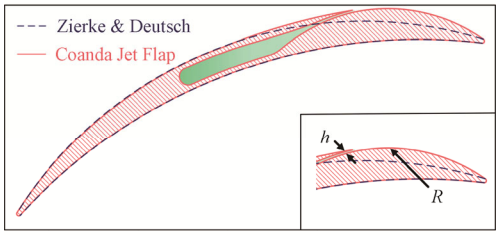

(b) Rear-jet

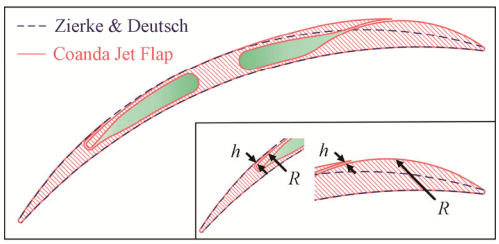

(c) Double-jet

Fig. 1 Zierke & Deutsch blade and Coanda jet flap 2D airfoil profiles

To realize a parametrization for the Coanda jet flap, three key geometric parameters including the Coanda surface radius (R) and two representative angles are utilized, as shown in Fig. 2. One of the two angles, i.e., θ, represents the position of the tangent intersection point between the Coanda curve and trailing edge (or leading edge), while the other angle, i.e., α, is that between the Coanda curve and modified suction surface. Selections of these parameters are referred to the study of Guendogdu [14], who indicates that the above three parameters have deterministic roles for the performance of a Coanda jet flap. It is worth mentioning that the ratio of the slot height (h) to R is less than 0.02 to ensure a good Coanda effect. Also, the jet mass flow ratio (m_j/m_1) is considered in the current design [13].

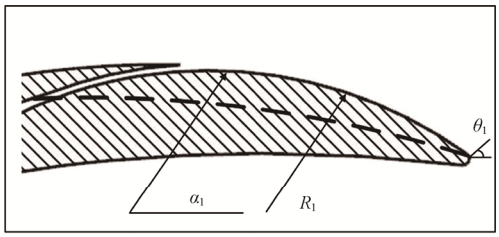

(a) Near trailing edge

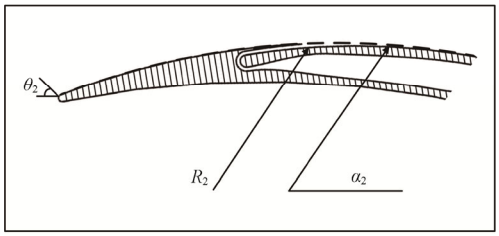

(b) Close to leading edge

Fig. 2 Coanda jet flap design parameters (a) near trailing edge, (b) close to leading edge

3. Numerical and Optimization Methods

3.1 Numerical schemes and validation

Flow field in the compressor described in Section 3 is obtained via numerically solving the compressible Navier-Stokes equations, which are expresses as:

$$\frac{\partial \rho}{\partial t}+\nabla\cdot(\rho U)=0 \tag{1}$$

$$\frac{\partial}{\partial t}(\rho U)+\nabla\cdot(\rho UU)=-\nabla p+\nabla\cdot\sigma_{\text{visc}} \tag{2}$$

$$\frac{\partial}{\partial t}\left[\rho\left(e+\frac{1}{2}U^2\right)\right]+\nabla\cdot\left[\rho\left(e+\frac{1}{2}U^2\right)U\right] =-\nabla\cdot(\rho U)+\nabla\cdot(\sigma_{\text{visc}}\cdot U)+\nabla\cdot(\kappa\nabla T) \tag{3}$$

where the viscous stress force (σ_{visc}), pressure (p) and internal energy (e) are defined as:

$$\sigma_{\text{visc}}=\frac{2}{3}\mu(\nabla\cdot U)+\mu\left[\nabla U+(\nabla U)^T\right] \tag{4}$$

$$p=\rho RT \tag{5}$$

$$e=C_vT \tag{6}$$

The specific heat under constant volume (C_v) is:

$$C_v=\frac{R}{\gamma_i-1} \tag{7}$$

To solve the above governing equation set, the

Reynolds-Averaging strategy is employed, and the shear stress transport (SST) k-ω turbulence model in conjunction with the correlation-based γ-Re_θ transition model are utilized. All simulations are performed using the commercial flow solver ANSYS/CFX, where the advection terms and the diffusion terms are discretized via second-order upwind and central difference schemes respectively.

Fig. 3 shows the computational domain of the compressor cascade, where only one single blade passage is modelled under the translationally periodic condition. The inlet and outlet are located at $2C_{ax}$ (C_{ax} is the blade axial chord) upstream and $2C_{ax}$ downstream of the blade leading and trailing edges respectively. The computational mesh is generated based on the H-O-H topology via the Numeca/IGG software package. Details of the grid near the blade are presented in Fig. 3. The non-dimensional wall distance y^+ is lower than 1 to satisfy the requirement of the turbulence model.

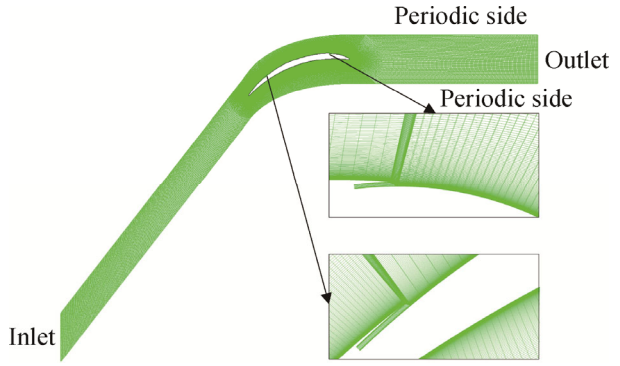

Fig. 3 Computational domain and grid scheme

For boundary conditions, the velocity corresponding to a Mach number of 0.6 and a total temperature of 288.15 K are applied at the inlet, and an average static pressure is set at the outlet. When Coanda jet flap is considered, mass flow rate and flow angle values are specified at the slot inlet. Meanwhile, the turbulent intensity of both the mainstream flow and the Coanda jet flow are equal to 5%. Meanwhile, all solid walls of the computational domain are set to be non-slip and adiabatic.

In order to verify the grid independence, computational grids with difference grid cell number are first generated to simulate the compressor cascade flow. Two parameters, including total pressure loss coefficient (ω) and static pressure coefficient (C_p), are utilized. Their definitions are formulated in Eqs. (8) and (9). Predicted ω is shown in Fig. 4. It can be seen that when the grid cell number is larger than 1.9×10^5, no significant change in ω is observed. Therefore, this level of grid number is employed in the following numerical simulations. In addition, Fig. 5 compares calculated static pressure

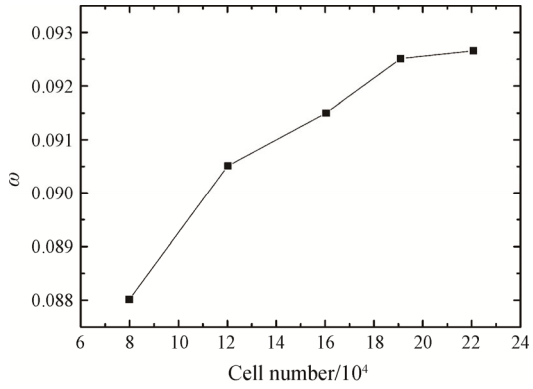

Fig. 4 Grid dependency study

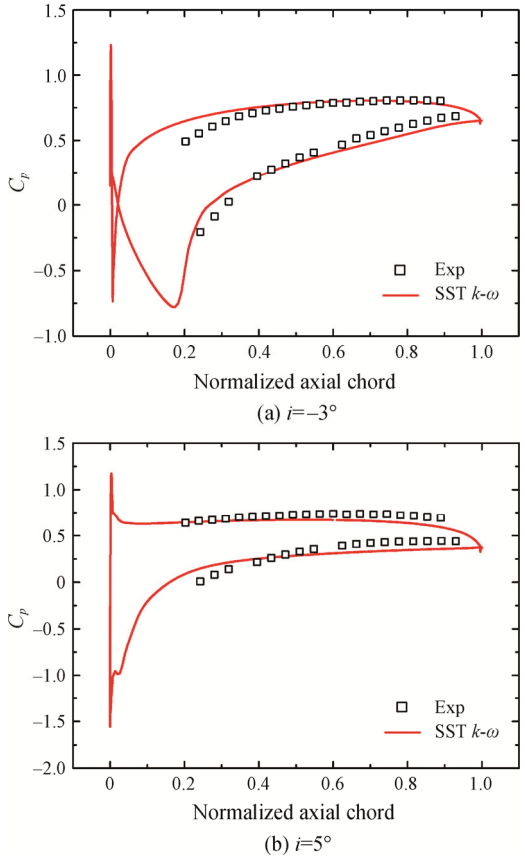

Fig. 5 Static pressure coefficient distributions at the incidence angle of (a)–3°, (b) 5°

coefficient (C_p) on the blade surface and measured data. Two inlet incidence angles of –3° and 5° are involved. The prediction can capture the similar values and changing trends of C_p as the experiments. This indicates that the numerical simulation has good predictive accuracy.

$$\omega = \frac{p_{t1} - p_{t2}}{p_{t1} - p_1} \tag{8}$$

$$C_p = \frac{p_i - p_1}{p_{t1} - p_1} \tag{9}$$

3.2 Optimization strategy

3.2.1 Back propagation neural network and model validation

Optimization design is always clumsy and time-consuming in turbomachinery field due to high-dimensional issues. Therefore, low fidelity models are gradually employed in current turbomachinery design system. These methods need not to solve the governing equations directly, while they can predict the objectives in a faster and more convenient way by using surrogate models such as the Artificial Neural Network (ANN), the Response Surface Model (RSM) and the Kriging model [17]. An ANN model termed as Back Propagation Neural Network is adopted in this paper to determine the geometric parameters of the Coanda jet.

The superiority of the BPNN lies in a fact that the weight and bias factors to build the network can be initialized with less random values. The input vector composed of training samples is mapped towards the input layer to simulate the signal propagation, and this process is called the forward training phase. It should be mentioned that results obtained by this initial network model cannot provide accurate output parameters. To further improve the model accuracy, the error between predicted output by the model and the expected output is back-propagated to the network to adjust the weight and bias factors. Those factors are updated repeatedly until satisfying a convergence criteria. This process is called the backward learning stage.

As mentioned in Section 1, the design variables for the jet flap include θ, α, R, and m_j/m_1 (Coanda jet mass flow ratio), and they are input parameters for the BPNN. Correspondingly, the output parameter is the optimization objective, i.e., the total pressure loss coefficient (ω). Based on this, the schematic diagram of the BPNN is illustrated in Fig. 6. In order to validate the BPNN, some training samples are first selected and they are listed in Tables 2 and 3. The performance value predicted by the BPNN model and CFD method are compared in Fig. 7. It can be seen the averaged relative error of the BPNN

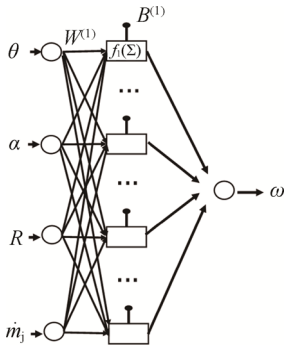

Fig. 6 Overall structure of BPNN

Table 2 Training samples for the Coanda jet flap near the trailing edge

Level	Value			
–	θ/(°)	α/(°)	R/mm	m_j/m_1
1	36	56	50	0.5%
2	38	58	54	0.7%
3	40	60	58	0.9%
4	42	62	62	1.1%
5	44	64	66	1.3%
6	46	66	70	1.5%

Table 3 Training samples for the Coanda jet flap close to the leading edge

Level	Value			
–	θ/(°)	α/(°)	R/mm	m_j/m_1
1	70	66	156	0.5%
2	72	68	158	0.7%
3	74	70	160	0.9%
4	76	72	162	1.1%
5	78	74	164	1.3%
6	80	76	166	1.5%

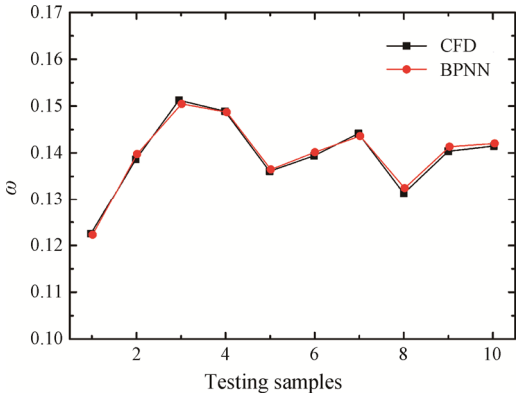

Fig. 7 Comparison of ω predicted by CFD and BPNN model

prediction is smaller than 1%. Thus, this BPNN model is accurate enough to predict the Coanda jet effect on the performance of the studied compressor airfoil.

3.2.2 Genetic algorithm and optimization flow-chart

Based on the BPNN established above, the genetic algorithm (GA) is adopted to determine the optimal solution. The GA method can avoid local optimization solution, which is commonly encountered in traditional gradient-based optimization approaches. The fundamental principle of the GA is to generate a randomly initial population and then evaluate the fitness of each individual in the population. Then the high fitness individuals are screening out and a new generation is generated based on the probability distributed

intersection and mutation of genomes. The optimization is terminated when a satisfactory fitness level is reached.

Figure 8 shows the flowchart of optimization process. The parameterization of the Coanda jet flap is introduced in Section 1. A design vector is then determined based on the changing range of the design parameters to ensure enough design samples. In addition, a uniform distribution testing method is adopted to design trailing samples and testing samples and the value levels for R, θ, α and m_j/m_1 in training database and testing database are six and five respectively. For the current study, changing ranges of the Coanda jet slot near the trailing edge (rear jet) for R, θ, α and m_j/m_1 are [50 mm, 90 mm], [30°, 60°], [40°, 70°], [0.5%, 1.5%], and the Coanda jet slot near the leading edge (front jet) for R, θ, α and m_j/m_1 are [154 mm, 168 mm], [64°, 78°], [70°, 80°], [0.5%, 1.5%] respectively. Performance of each design sample is acquired using the CFD solver introduced in Section 3.1. Then, the initial weights and biases of BPNN surrogate model mentioned above are optimized by GA to improve convergence speed and reduce calculation amount. Meanwhile, the BPNN surrogate model is used to learn training samples database and predict the objective parameter. The prediction accuracy is evaluated on the basis of testing database. Finally, the optimal Coanda jet flap is generated by this new optimization algorithm.

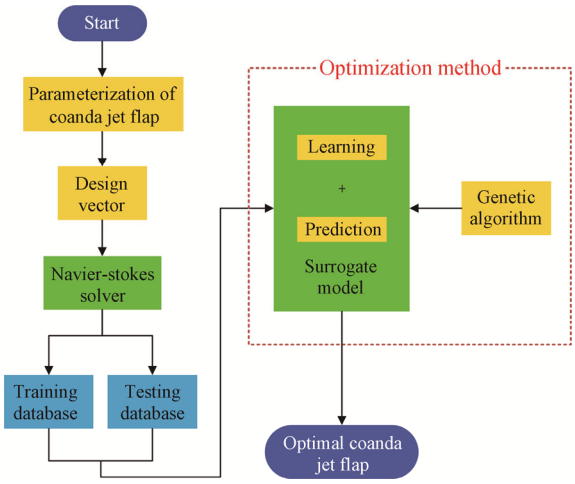

Fig. 8 Flowchart of optimization process

4. Results and Discussion

4.1 Flow field in the reference cascade

As mentioned before, to determine some initial Coanda jet flap configurations, the flow field of the highly loaded compressor cascade at the incidence angle (i) of 5° under various inlet Mach number (Ma_{in}) conditions are first investigated. Predicted results using CFD are shown in Fig. 9.

It can be first seen that serious boundary layer flow separation is generated near the suction surface at this positive incidence angle condition. This is mainly attributed to the relative large blade camber angle. The separation is located at 30.6%C_{ax} when Ma_{in} is 0.1, while it is moved forward to 18.2%C_{ax} when Ma_{in} is increased to 0.6. Thus, the higher the Ma_{in}, the closer to the leading edge for the separation location.

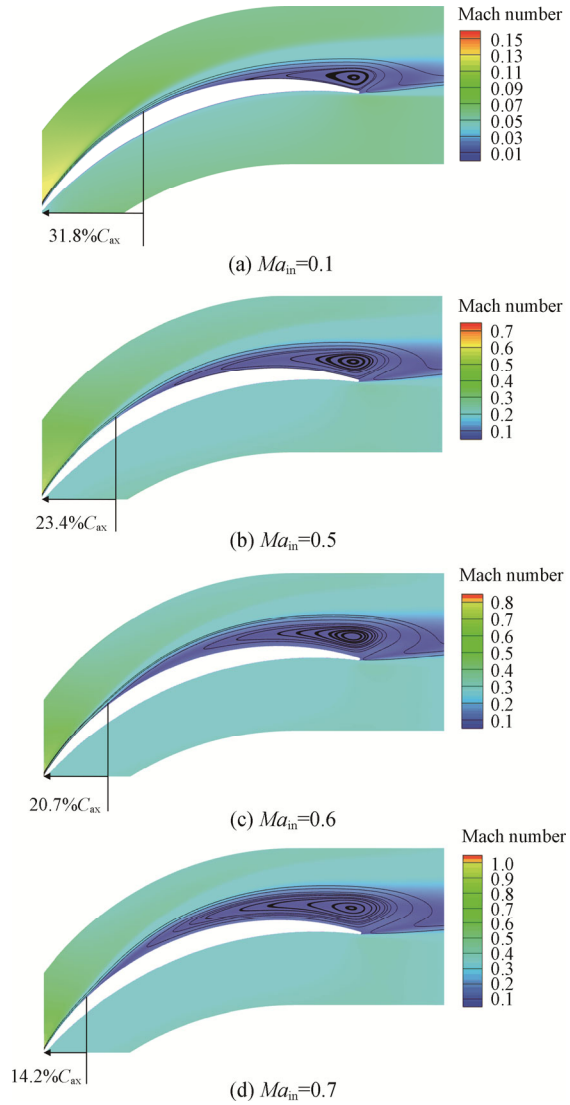

Fig. 9 Mach number contours and streamlines at the incoming Mach number of (a) 0.1, (b) 0.5, (c) 0.6, (d) 0.7

4.2 Optimized jet flap configurations and performance analysis

Based on the flow filed in Fig. 9, the three configurations of the Coanda jet in Fig. 1 are optimized. Optimal results, as termed as front-jet, rear-jet and double-jet here, are finally obtained and relevant values of the four design parameters are listed in Table 4. Also, the optimal results are illustrated in Fig. 10 to make

things clear to readers. To quantitatively evaluate the Coanda jet effect on the compressor airfoil performance, the total pressor loss and static pressure rise coefficients will be further employed. It should be mentioned that, the inlet total pressure should be modified to consider the injection flow effect, as indicated by Eq. (12). Therefore, ω and ΔP_s are redefined as Eqs. (10)–(11). Meanwhile, relative changes in ω and ΔP_s as defined in Eqs. (13)–(14) respectively.

$$\omega = \frac{p_{t1j} - p_{t2}}{p_{t1} - p_1} \tag{10}$$

$$\Delta P_s = \frac{p_2 - p_1}{p_{t1} - p_1} \tag{11}$$

$$P_{t1j} = \frac{m_1 p_{t1} + m_j p_{tj}}{m_1 + m_j} \tag{12}$$

$$d\omega = \frac{\omega_j - \omega}{\omega} \tag{13}$$

$$d(\Delta P_s) = \frac{\Delta P_{sj} - \Delta P_s}{\Delta P_s} \tag{14}$$

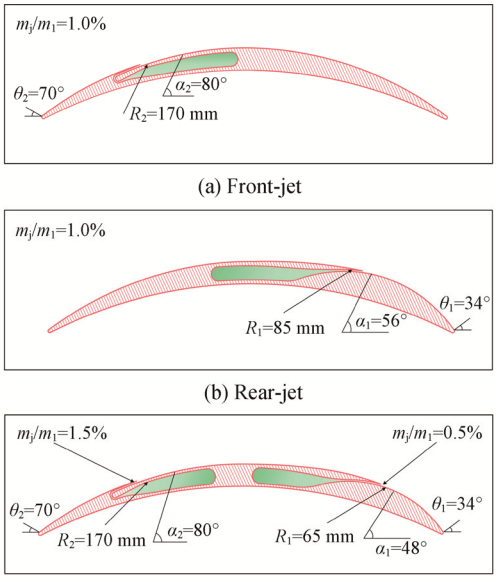

Fig. 10 2D optimal Coanda jet flap Airfoil

Table 4 The values of parameters of the optimal three types

Parameter	Front-jet	Rear-jet	Double-jet
θ_1/(°)	–	34	34
α_1/(°)	–	56	48
R_1/mm	–	85	65
m_j/m_1	–	1%	0.5%
θ_2/(°)	70	–	70
α_2/(°)	80	–	80
R_2/mm	170	–	170
m_j/m_1	1.5%	–	1.5%

In order to first investigate the effects of three optimal Coanda jet flaps on controlling the boundary layer flow separations, Fig. 11 shows the distributions of streamlines and contours of Mach number for the compressor with and without Coanda jet flap. Results are

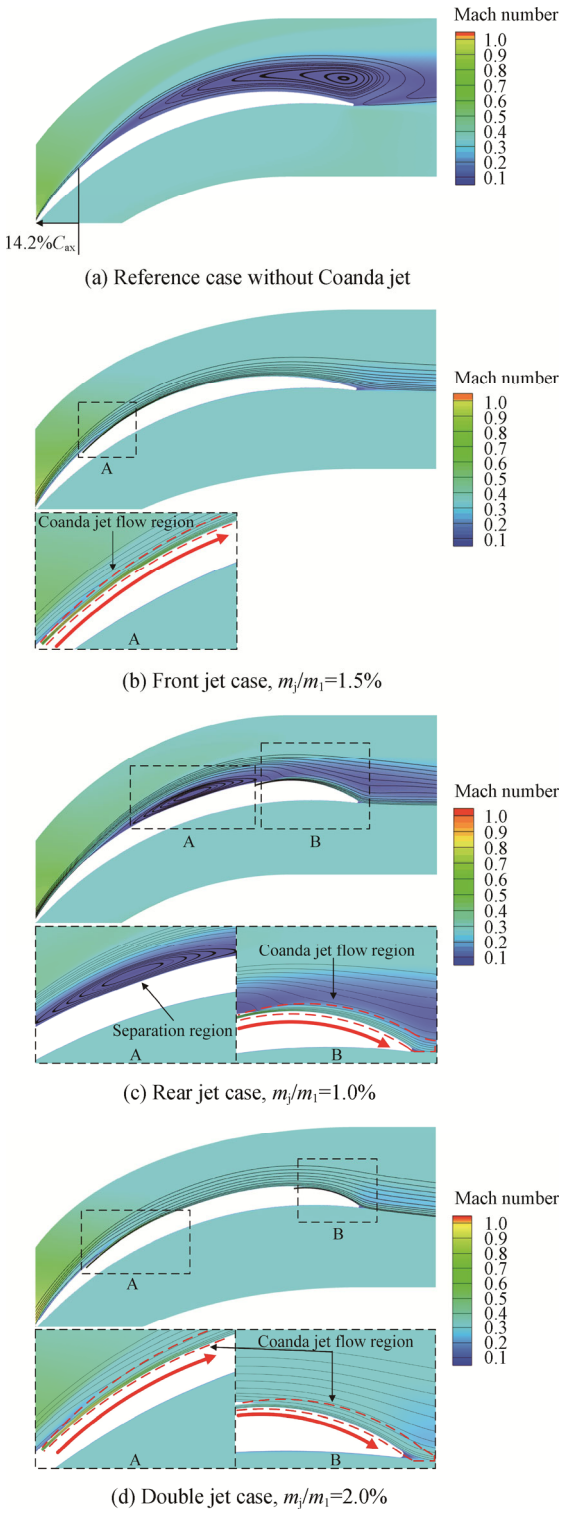

Fig. 11 Streamlines and Mach number contours at the incidence angle of 5°

obtained for i=5° and Ma_{in}=0.6. For the reference cascade, there is a serious flow separation which is produced at14.2%C_{ax} of the suction surface, as shown in Fig. 11(a). The momentum of the flow near the Coanda surface is enhanced dramatically after introducing the Coanda jet, as indicated by the Ma values near the Coanda jet slot. For the front-jet case, there is tiny little flow separation region near the trailing edge with the Coanda jet mass flow ratio being 1.5% as shown in Region A of Fig 11(b). For the rear-jet case, the large flow separation region is generally reduced when the Coanda jet mass flow ratio is 1%, see Fig. 11(c), while, boundary layer flow separation is still attached to the suction surface in Region A and Region B. For the double-jet case, the separation region near the suction surface is completely controlled with the Coanda jet mass flow ratio of 2% in Fig. 11(d).

4.3 Effects of geometric parameter of the Coanda jet flap

According to the above analysis, the double-jet has the best effect on inhibiting the separation near the suction surface. In order to minimize the difference of flow field between the reference airfoil and the modified airfoil, the changes in the suction surface profile near the front jet slot are relatively small. This means that the varying range of geometric parameters of the front jet slot is small. In addition, since the variation of the parameter α has less influence on the modified airfoil performance [17], hence only the effects of the parameters θ and R of the jet slot near trailing edge in the double-jet case are investigated in this section.

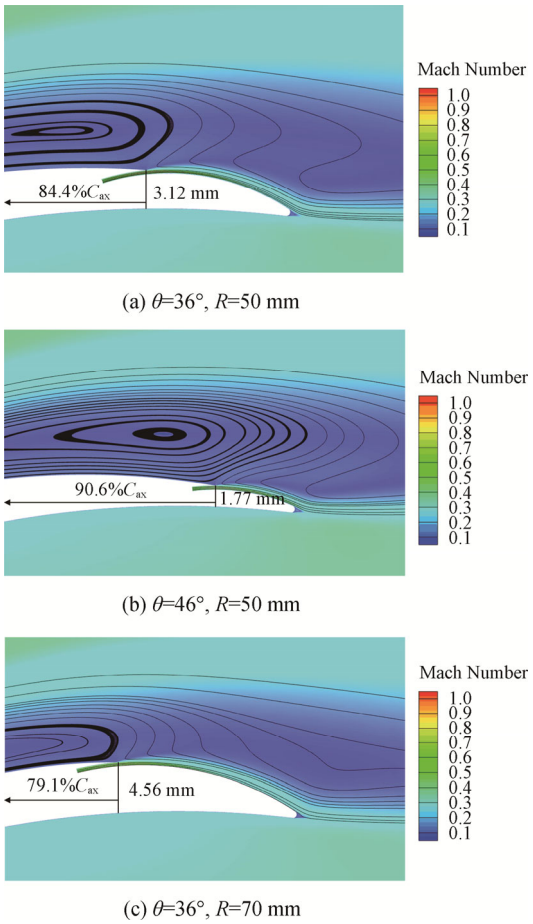

Fig. 12 Streamlines and Mach number contours at the slot region near the trailing edge (m_j/m_1=1.0%)

Fig. 12 shows streamlines and Mach number contours at the slot region near the trailing edge. The incidence angle and jet mass flow ratio are 5° and 1% respectively. Two phenomenon can be observed from the figure following conclusions can be draw accordingly. The first is that smaller θ and R result in thicker blade profile close to the trailing edge, and this is beneficial to improve the aerodynamic performance. Also, both the geometric parameters θ and R have determined the jet slot positions. In other words, the jet slot position upstream the initial separation onset position is beneficial to control the boundary layer flow separation. Both effects make the well-designed Coanda jet flap more robust and efficient in controlling the highly loaded compressor flows.

4.4 Effects of mass flow rate of the Coanda jet flap

In order to quantitatively evaluate the Coanda jet effect on the compressor airfoil performance, and tclarify the mechanism of the Coanda jet effect on controlling the aerodynamic loss. The total pressor loss and static pressure rise coefficients (ω and ΔP_s) defined in Eqs. (10)–(11) are further analysed. Their relative changes, i.e., dω and d(ΔP_s) as formulated in Eqs. (13)–(14), are plotted in Fig. 13.

It can be observed that compared with the reference airfoil, the total pressure loss coefficients are reduced and the static pressure rise coefficients are increased for the three Coanda jet flap cases when jet mass flow ratio is 0, of which the most successful single intervention is the rear-jet case.

Meanwhile, the total pressure loss coefficient of the front-jet, rear-jet and double-jet is the lowest when the Coanda jet mass flow ratio is 1.5%, 1% and 2% respectively. Moreover, double-jet configuration has the best ability to control the boundary layer flow separation. It can reduce the total pressure loss coefficient by 52.5%, and increase the static pressure rise coefficient by 25.7% when the Coanda jet mass flow ratio is equal to 2%. To interpret this phenomenon, the flow fields in the double-jet case as illustrated by Fig. 14 under different jet mass flow ratios are presented in Fig. 15.

The large flow separation bubble is generally reduced with increasing the Coanda jet mass flow ratio of the jet slot near the leading edge, and there is a slight difference

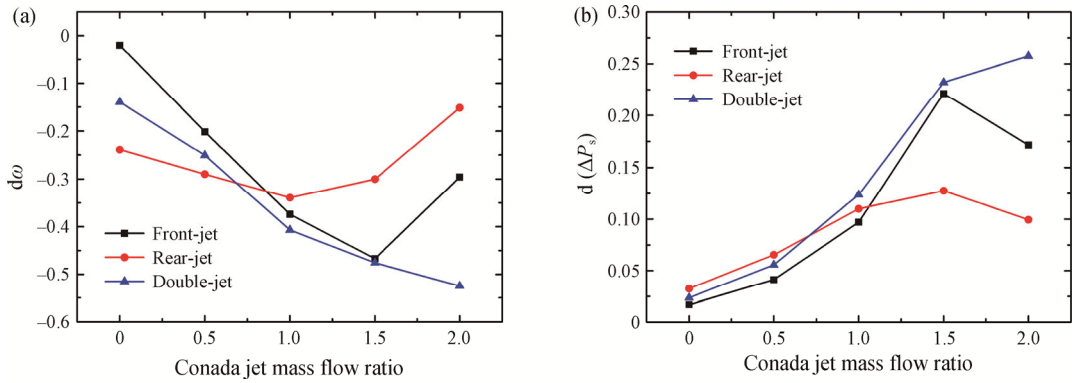

Fig. 13 Performance of three types of Coanda jet flap at variable mass flow ratios

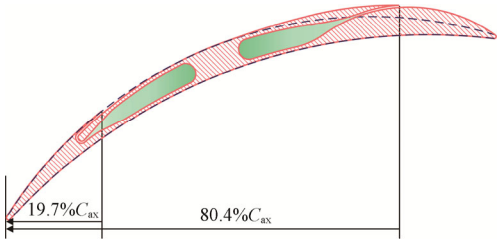

Fig. 14 Axial relative position of the Coanda jet slot

on controlling separation on the suction surface when increasing the Coanda jet mass flow ratio of the jet slot near the trailing edge. The aerodynamic performance of the compressor airfoil is enhanced dramatically with the Coanda jet at the initial onset of the separation region when the jet mass flow ratio of the slot close to the leading edge increases to 1.0% and 1.5%. On the other hand, the Coanda jet slot near the leading edge plays the key role in controlling the boundary layer flow separation when compared with the Coanda jet slot close to the trailing edge.

Here the effect of the double-jet case on controlling the flow separations is investigated with variable incidence angles, as shown in Fig. 16. It contains the variations of the total pressure loss coefficients under the various incidence angles at nine combinations of Coanda jet flow ratios. No mass flow ratio is required for the Coanda jet slot near the leading edge at the smaller incidence angles, which is attributed to the boundary layer flow separation occurred on the suction surface close to the trailing edge. The reduction in the total pressure loss coefficients reaches to the maximum level with 1.5% mass flow ratio near the leading edge and 0.5% mass flow ratio close to the trailing edge when the incidence angle increases to 3° and 5°. Thus, the red line represents the best combination of the Coanda jet flow ratio with variable incidence angles. This provides a quantitative evaluation of the Coanda jet flap and offers a guideline for future adaptive flow control techniques.

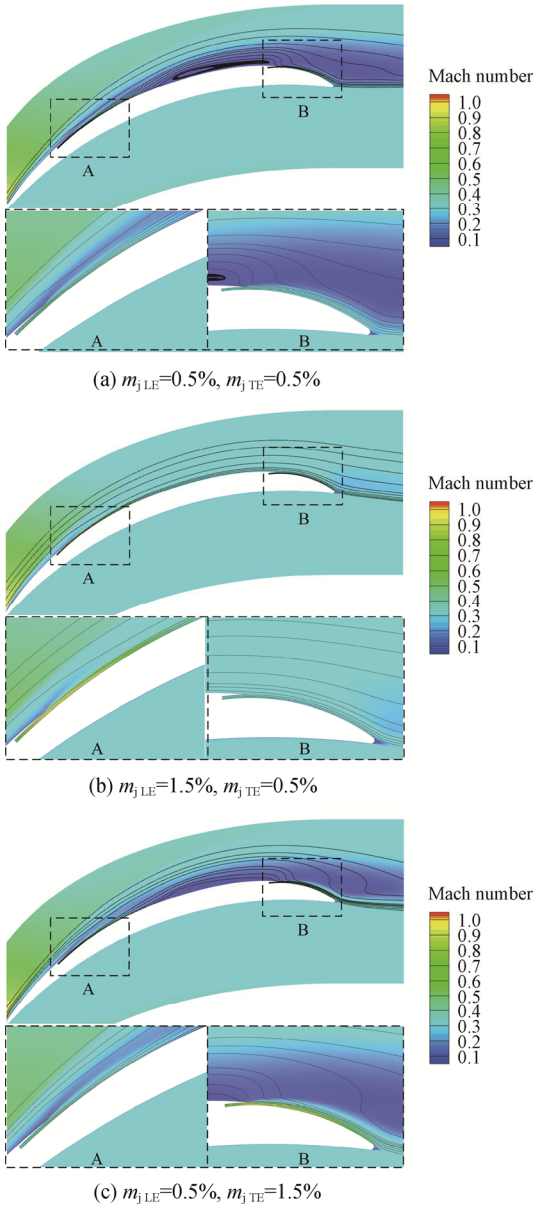

Fig. 15 Streamlines and axial Mach number contours at variable combinations of mass flow ratios

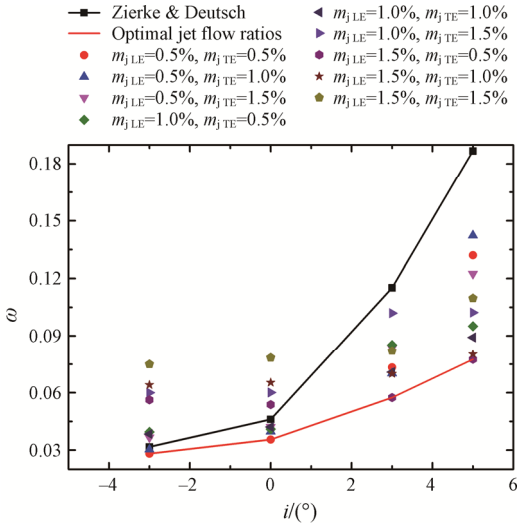

Fig. 16 Distributions of total pressure loss coefficients at different incidence angles combined with various jet mass flow ratios

5. Conclusions

In order to alleviate and eliminate the flow separations in highly loaded compressors, the flow control technique based on the Coanda jet flap is investigated. Three types of the Coanda jet flap configurations are obtained via an optimization scheme coupled with back propagation neural network (BPNN) and Genetic algorithm (GA). Their effects on the flow field and performance of a highly loaded compressor are analyzed based on numerical simulations that are validated using experimental method. The impacts of some key geometric parameters, including the Coanda surface radius (R) and two representative angles (θ and α), and injection mass flow rates (m_j/m_1) are also clarified. The major conclusions are summarized as follows:

(1) The three optimized Coanda jet flaps based on the GA-BP neural network algorithm, include a front-jet with θ=70°, α=80°, R=170 mm and m_j/m_1 =1.5%, a rear-jet with θ=34°, α=56°, R=85 mm and m_j/m_1 =1%, and a double-jet with θ_1 =34°, α_1 =48°, R_1 =65 mm, m_j/m_1 =0.5%, θ_2 =70°, α_2 =80°, R_2 =170 mm and m_j/m_1 =1.5%. The double-jet has the best effect on controlling the boundary layer flow separation, and it can reduce and increase the total pressure loss coefficient and the static pressure rise coefficient by 52.5% and 25.7% respectively when m_j/m_1 equals to 1.5% and 0.5% at leading and trailing edge jet slot respectively.

(2) The geometric parameters θ and R have a major impact on the performance of the Coanda jet flap, which determines the blade thickness and the jet slot positions. A smaller value of θ in conjunction with a larger value of R, i.e., a thickener airfoil with a jet slot upstream the flow separation point results in the improved aerodynamic performance. In other words, a thickener airfoil aids to accelerate the air flow. Hence, it can enhance the boundary layer momentum and increase the ability of the flow to resist the adverse pressure gradient.

(3) The jet slot near the leading edge of the double-jet is mostly sensitive to the variations of the Coanda jet mass flow ratios. It is observed that higher injection mass flow ratios have stronger ability to control the separation adhere to almost the whole suction surface. Also, the total pressure loss coefficients can be significantly reduced by appropriately adjusting the combinations of Coanda jet mass flow ratios between two jet slots for the double-jet at the variable of incidence angles. This offers a guideline for adaptive flow control techniques in future applications of the Coanda jet flap.

Acknowledgements

The authors would greatly thank the supports from the grants of the National Natural Science Foundation of China (Nos. 51922098, 51790510, and 51636001), the National Major Project of Aeroengine and Gas Turbine (2017-II-0004-0017 and J2019-II-0020-0041).

References

[1] Deutsch S., Zierke W.C., The measurement of boundary layers on a compressor blade in cascade: part 1-a unique experiment facility. Journal of Turbomachinery, 1987, 109(4): 520–526.

[2] Lee N.K.W., Greitzer E.M., Effects of endwall suction and blowing on compressor stability enhancement. Journal of Turbomachinery, 1990, 112(5): 133–144.

[3] Zhou Y., Liu H.X., Zou Z.P., Ye J., Boundary layer separation control on a highly-loaded, low-solidity compressor cascade. Journal of Thermal Science, 2010, 19(2): 97–104.

[4] Zheng X., Li Z., Blade-end treatment to improve the performance of axial compressors: an overview. Progress in Aerospace Sciences, 2017, 88: 1–14.

[5] Li Y.H., Wu Y., Zhou M., Su C.B., Zhang X.W., Zhu J.Q., Control of the corner separation in a compressor cascade by steady and unsteady plasma aerodynamic actuation. Experiments in Fluids, 2010, 48(6): 1015–1023.

[6] Dal M.A., Castelli M., Benini E., A retrospective of high-lift device technology. Engineering and Technology, 2012, 71: 1979–1984.

[7] Edward L., Clark J., An experimental study of jet-flap compressor blades. Journal of the Aerospace Sciences, 1959, 26(11): 698–702.

[8] Landsberg T.J., Krasnoff E., An experimental study of rectilinear jet-flap cascades. Journal of Basic Engineering,

1972, 94(1): 97–104.

[9] Inventions R., Aviation P.I., Constantin C, Gheorghiu, Ed. Albatros, Bucharest, 1979.

[10] Hill H.E., Ng W.F., Vlachos P.P., Guillot S.A., Bailie S.T., 2D parametric study using CFD of a circulation control inlet guide vane. 5th Joint ASME/JSME Fluids Engineering Conference, San Diego, California USA, 2007, FEDSM2007-372294.
DOI: 10.1115/fedsm2007-37294.

[11] Fischer S., Saathoff H., Radespiel R., Two-dimensional RANS simulations of the flow through a compressor cascade with jet flaps. Aerospace Science and Technology, 2008, 12(8): 618–626.

[12] Vorreiter A., Fischer S., Radespiel R., Seume J.R., Numerical investigations of the efficiency of circulation control in a compressor stator. Journal of Turbomachinery, 2012, 134(2): 021012.

[13] Fischer S., Müller L., Kožulović D., Three-dimensional flow through a compressor cascade with circulation control. Proceedings of ASME Turbo Expo 2012, Copenhagen, Denmark, 2012, GT2012-68593. DOI: 10.1115/gt2012-68593.

[14] Guendogdu Y., Vorreiter A., Seume J.R., Design of a low solidity flow-controlled stator with Coanda surface in a high-speed compressor. Proceedings of ASME Turbo Expo 2008: Power for Land, Sea and Air, Berlin, Germany, 2008, GT2008-51180.
DOI: 10.1115/gt2008-51180.

[15] Schwerdt L., Siemann J., Seume J.R., Active flow control implemented in a multi-stage high-speed axial compressor. PAMM, 2016, 16(1): 645–646.

[16] Zierke W., Deutsch S., The Measurement of boundary layers on a compressor blade in cascade volume 1 experimental technique, analysis and results. NASA Technical Report, CR-185118, 1989.

[17] Li Z., Zheng X., Review of design optimization methods for turbomachinery aerodynamics. Progress in Aerospace Sciences, 2017, 93: 1–23.